Molecular Cell, Volume *78*

Supplemental Information

Replicational Dilution of H3K27me3 in Mammalian Cells and the Role of Poised Promoters

Unmesh Jadhav, Elisa Manieri, Kodandaramireddy Nalapareddy, Shariq Madha, Shaon Chakrabarti, Kai Wucherpfennig, Megan Barefoot, and Ramesh A. Shivdasani

Jadhav et al, **Figure S1** (relates to **Figure 1**)

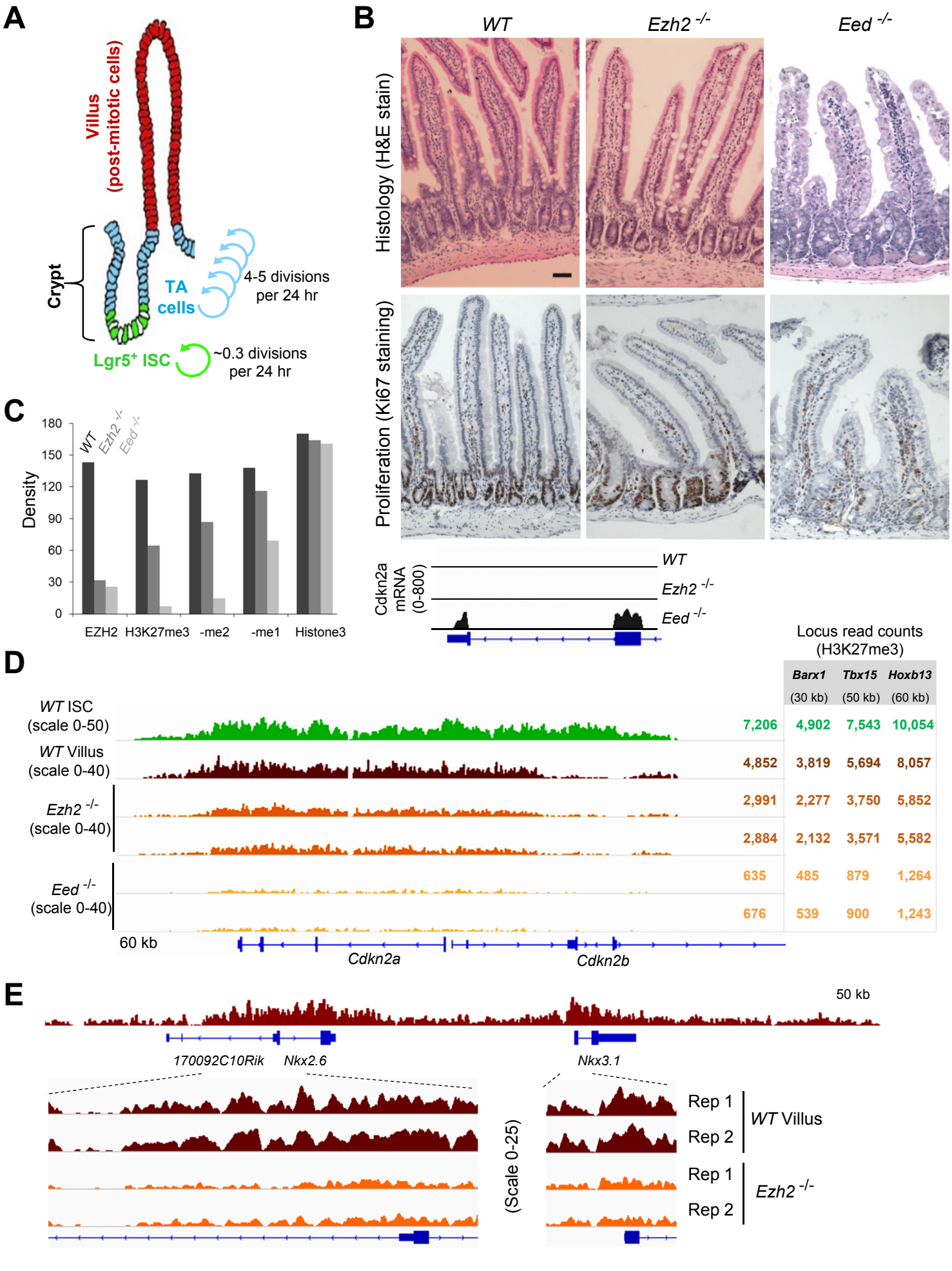

Figure S1. Differential effects of *Ezh2* and *Eed* deletion in intestinal epithelium. (relates to Figure 1)

A) Stereotypic organization of intestinal crypt-villus units: $Lgr5^{+}$ ISC reside at the crypt base and divide less frequently than their transit-amplifying (TA) cell progeny, which occupy most of the crypt. Villus cells, derived from these progenitors, are non-cycling and terminally differentiated.

B) Histology (top) and KI67 immunohistochemistry (bottom) of mouse duodenum (as an example of the whole small intestine) after *Ezh2* or *Eed* deletion. Epithelial structure and crypt cell proliferation are affected only after EED loss. mRNA levels (from RNA-seq) of a representative PRC2 target gene support these findings. Sections from at least 3 mice for each genotype were stained.

C) Levels of EZH2 and of methylated H3K27 forms in WT, $Ezh2^{-/-}$ and $Eed^{-/-}$ villus epithelium, quantified from immunoblots shown in Fig. 1B.

D) ChIP-seq data showing partial loss of H3K27me3 in $Ezh2^{-/-}$ and near-total loss in $Eed^{-/-}$ villus cells (2 replicates each), across the *Cdkn2a/2b* region. Numbers indicate ChIP-seq read counts over 60 kb and over regions of the indicated size in other PRC2 target loci.

E) H3K27me3 ChIP-seq data from mouse intestinal villus cells at *Nkx*-family (examples) genes, showing reproducible variation in H3K27me3 signals across the loci. This intra-locus variability, evident in independent replicates (Rep), is unlikely to reflect cellular heterogeneity because >90% of cells in adult duodenal villi are post-mitotic enterocytes. Rather, the variability may reflect (i) local variation in PRC2 activity, or (ii) the balance between methyltransferase (PRC2) and demethylase (KDM6) activities. The local variation is accurately preserved when regional H3K27me3 is reduced by ~60% in $Ezh2^{-/-}$ intestinal cells.

Jadhav et al, **Figure S2**
(relates to Figure 3, 4)

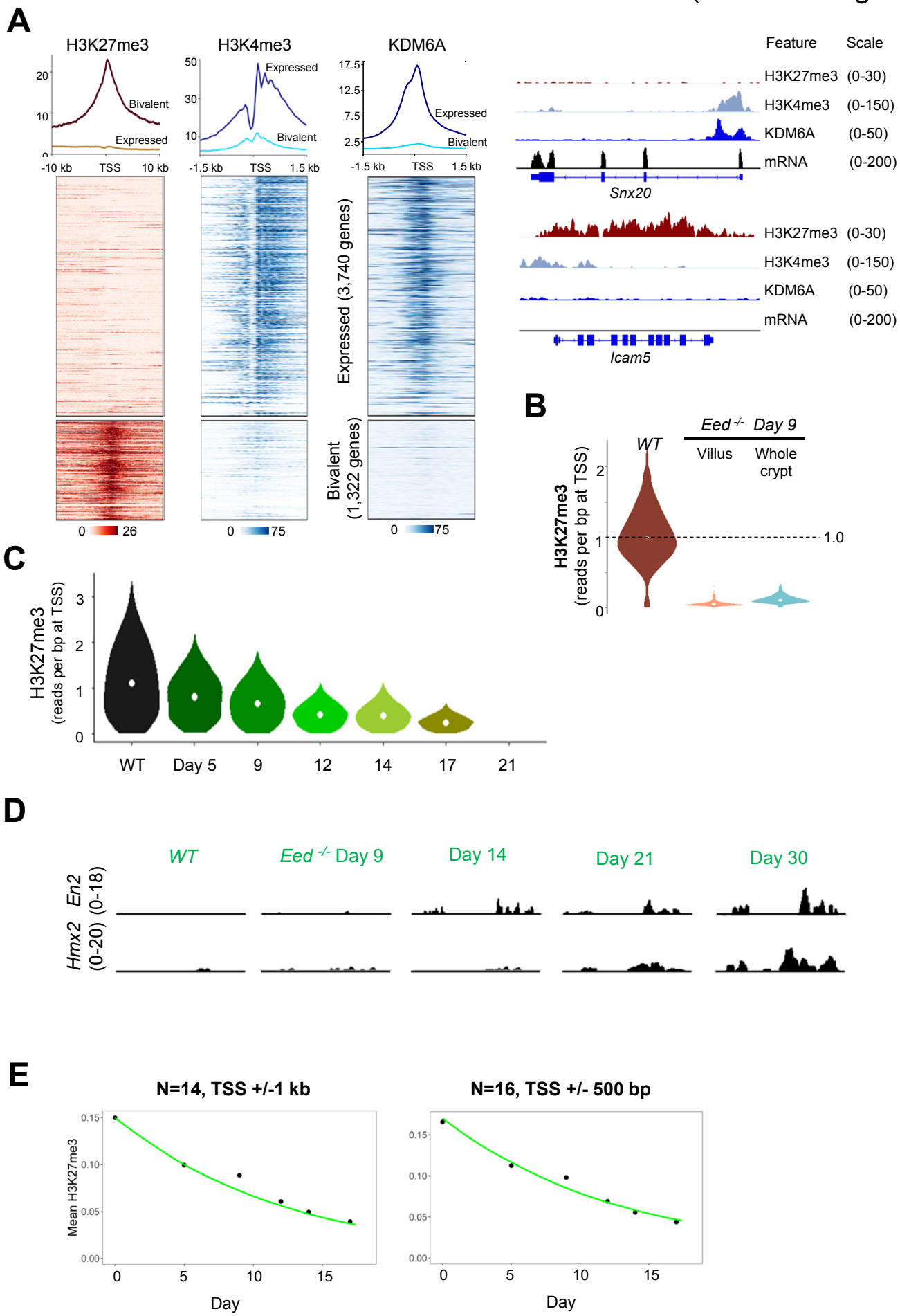

Figure S2. H3K27me3 decay in PRC2-null ISC and effects on gene expression. (relates to Figures 3 and 4)

A) Aggregate density profiles (top) and heatmaps (below) depicting ChIP-seq read distributions of H3K27me3, H3K4me3, and KDM6A around the TSSs of 1,322 silent bivalent (lower cluster) and 3,740 expressed (upper cluster) genes. KDM6A is present at expressed, and excluded from PRC2 target, promoters. IGV tracks for representative genes are shown to the right.

B) Quantitation of aggregate H3K27me3 ChIP-seq data at target genes, showing comparable loss of signal in *Eed*$^{-/-}$ whole crypts, which are dominated by TA cells (see Fig. S1A-B), and villus epithelium (2nd replicate of sample, similar to Fig. 1C).

C) Quantitation of H3K27me3 (ChIP-seq) at PRC2 target promoters in *Eed*$^{-/-}$ ISC, revealing slow depletion compared to post-mitotic villus cells or TA cells (whole crypt – see Fig. S2B).

D) IGV tracks of RNA-seq data at additional representative PRC2 target genes in Lgr5^{+} ISC purified by GFP flow cytometry at different times after initial CRE activation.

E) Evidence that the model for the rate of H3K27me3 decay in *Eed*$^{-/-}$ ISC gives the same results whether we consider each crypt to house 14 or 16 Lgr5^{+} cells, and whether H3K27me3 near TSSs is measured over a 500-bp or 1-kb interval.

Jadhav et al, **Figure S3**
(relates to Figure 5)

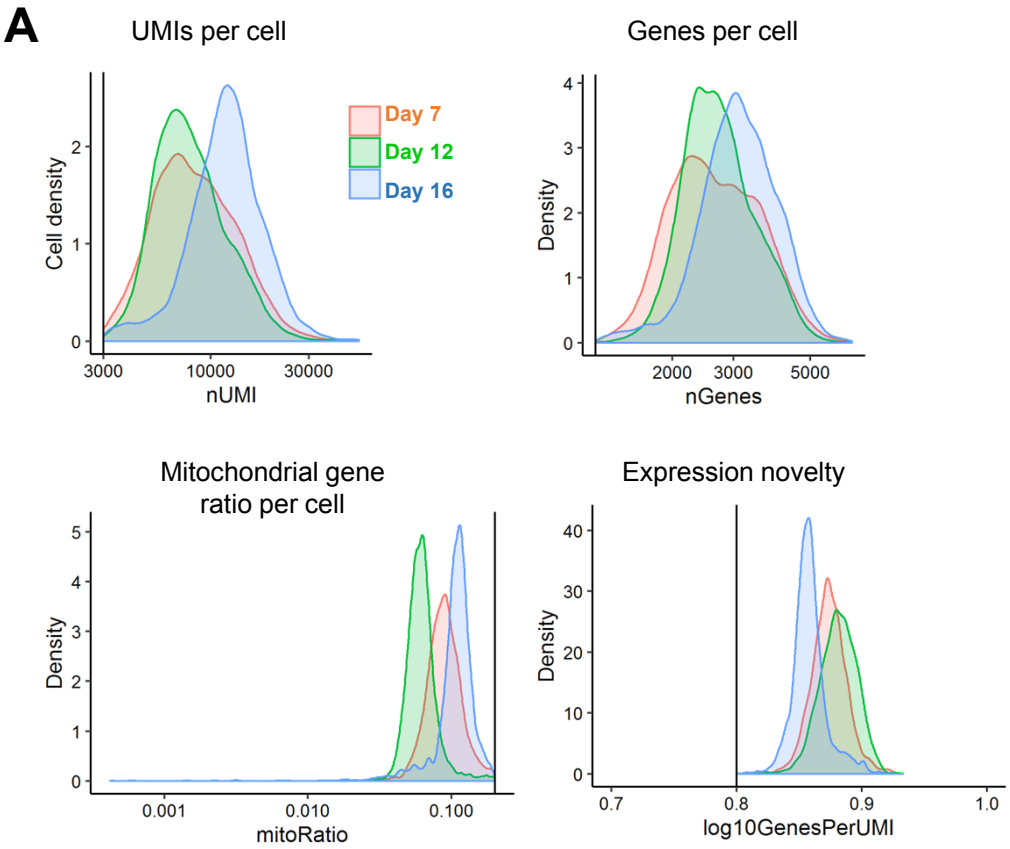

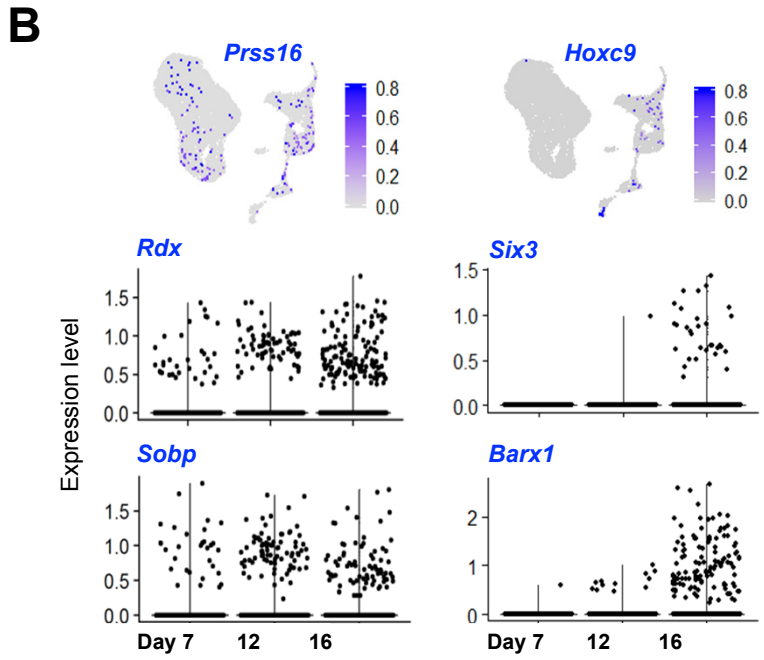

Figure S3. Single-cell transcriptomics of *Eed*$^{-/-}$ ISC over time. (relates to Figure 5)
A) Cell density plots from scRNA-seq data, showing the filtering criteria we applied to isolate informative cells: those with >3,000 unique molecular identifiers (UMIs) per cell, >1,200 genes detected per cell, mitochondrial ratio <0.2 per cell, and expression novelty > 0.8. The final analysis included 11,123 cells in all – 3,749 cells from day 7; 4,641 cells from day 12; and 2,733 cells from day 16.
B) Additional UMAP and violin plots showing early- and late-activated PRC2 target genes in single *Eed*$^{-/-}$ ISC.

Jadhav et al, **Figure S4**
(relates to Figure 6)

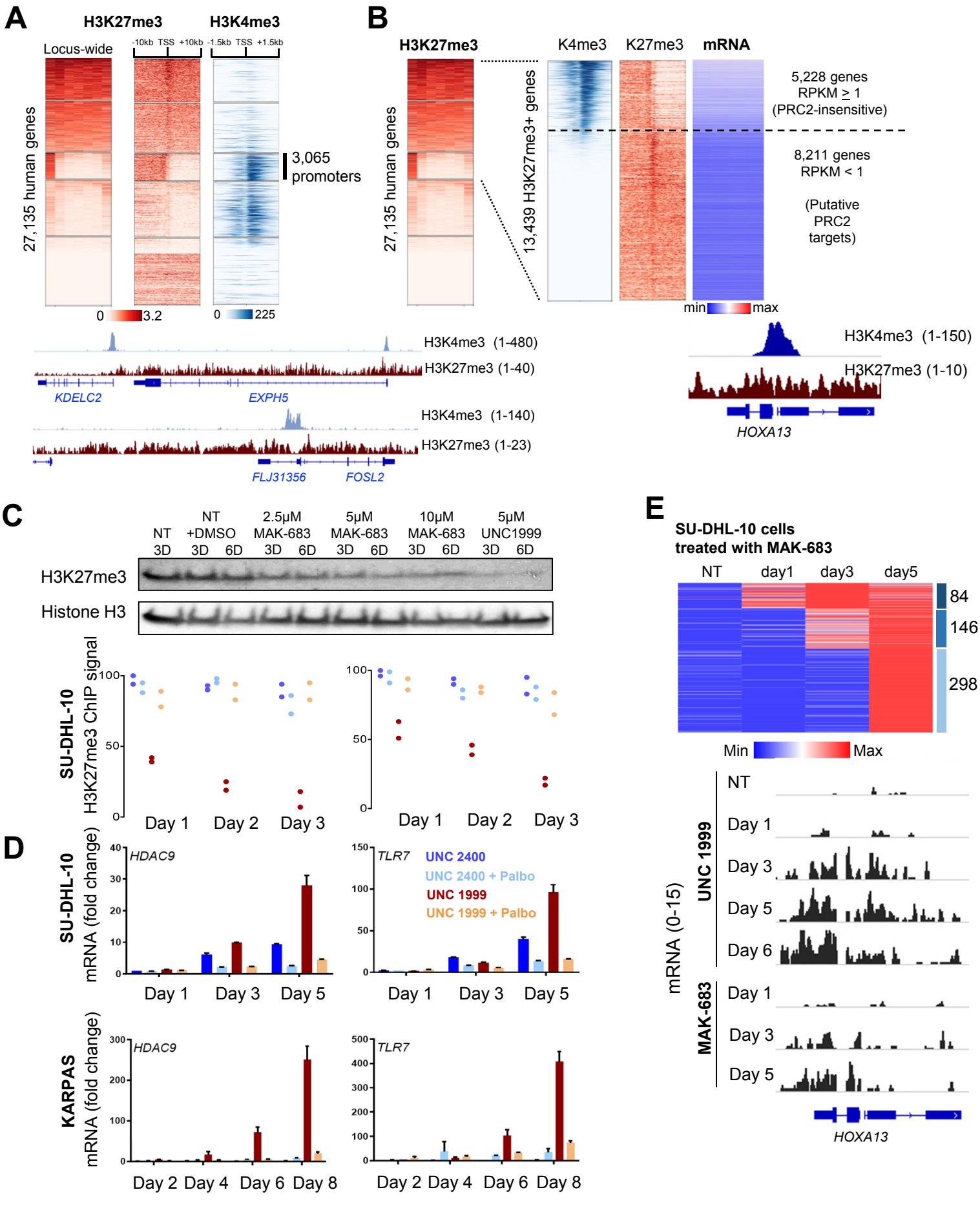

Figure S4. Bivalent genes, H3K27me3 decay, and PRC2 target gene reactivation in human lymphoma cells. (relates to Figure 6)

A) H3K27me3 distribution in SU-DHL-10 cells at 27,135 human RefSeq genes, represented over gene bodies (divided in 5 equal-sized bins) and 2-kb regions upstream of the TSS (1st column) and downstream of the transcription end site (last column). Genes are clustered by *k*-means (*k* =5) based on H3K27me3 ChIP signal strength and arranged in order of decreasing signal (left). H3K27me3 signal at TSSs ±10 kb (middle) and H3K4me3 signal at TSSs ±1.5 kb (right) revealed 3,065 genes with no H3K7me3 over the locus and high promoter H3K4me3, suggesting non-repressed genes. IGV tracks show heavy H3K27me3 marking at *EXPH5* and *FOSL2*, which also carry the active promoter mark H3K4me3 and are accordingly considered bivalent. *KDELC2* represents an expressed gene with H3K27me3 at the promoter but not the gene body.

B) Heatmaps showing 13,439 genes from top 3 clusters (high H3K27me3), arranged by decreasing promoter H3K4me3 signal. The 5,228 genes with highest promoter H3K4me3 lacked H3K27me3 on the gene body and were expressed (RPKM > 1). In contrast, 8,211 silent (RPKM <1) genes qualify as putative PRC2 targets. *HOXA13* is one such gene, showing high H3K27me3 across the locus and H3K4me3 at the promoter.

C) Immunoblots showing progressive loss of H3K27me3 over time upon exposure to various concentrations of the EED inhibitor MAK-683 or EZH2 inhibitor UNC1999. Below are additional examples of H3K27me3 decay (ChIP-qPCR data at selected promoters) in SU-DHL-10 cells captured on different days after treatment with UNC1999 or its inactive analog UNC2400, with or without palbociclib, in biological duplicates.

D) Additional examples of PRC2 target gene activation (qRT-PCR data) in SU-DHL-10 (top) and KARPAS-422 (bottom) cells captured on different days after treatment with UNC1999 or its inactive analog UNC2400, with or without palbociclib, in biological triplicates.

E) RNA-seq data (log_2 RPKM+1) from SU-DHL-10 cells treated with the EED inhibitor MAK-683, showing delayed and progressive activation of PRC2 target genes. Data represent single replicates of untreated cells and cells on 3 different days after the start of drug treatment. The IGV tracks below demonstrate gradual activation of the bivalent gene *HoxA13* upon treatment of SU-DHL-10 cells with UNC1999 (top) or MAK-683 (bottom).